

MICROCRACK AND FATIGUE BEHAVIOR OF HIGH-PERFORMANCE FIBER-REINFORCED CONCRETE UNDER CYCLIC COMPRESSIVE LOADING

NIKLAS SCHÄFER* AND ROLF BREITENBÜCHER*

* Ruhr-University Bochum, Chair of Building Materials
Universitätsstraße 150, 44801 Bochum, Germany
e-mail: Niklas.Schaefer@rub.de, www.baustoffe.ruhr-uni-bochum.de

Key words: High-strength Concrete, Fiber Reinforced Concrete, Composites, Durability

Abstract: The ongoing trend to create slender constructions makes the use of high-performance building materials indispensable. One problem with lightweight construction is an increasing vulnerability to fatigue loads caused by time-variant loadings, which may ultimately lead to earlier fatigue failure. Examples include bridge girders, onshore and offshore installations, which are affected by time-variant loadings such as traffic, wind, and waves simultaneously. The design of filigree and slender constructions implies an increased sensitivity to vibrations due to various external loads. This, however, may cause higher fatigue loads under cyclic stresses, which may further lead to damage or even failure of the concrete components before the maximum static strength is achieved. High-performance concretes have a denser matrix in comparison to normal-strength concrete and associated with this is a very brittle material behavior in the event of failure. Steel fibers can positively influence this brittle failure behavior and improve the ductility of the high-strength matrix. The extent to which this can have a beneficial effect on fatigue behavior has not yet been sufficiently researched experimentally. In this context, systematic investigations were carried out to gain knowledge about the influence of two different types of microfibers (steel and carbon). The fibers were selected in such a way that they can bridge microcracks in the range of <50 micrometers. To be able to investigate and compare the influence of the fibers on the fatigue behavior and the damage progress, the strain in the axial direction and an extensive microscopic evaluation of the microcrack behavior were carried out. For this purpose, sections were taken from the specimens according to defined numbers of load cycles, and thick sections were prepared. These thick sections were examined microscopically and evaluated concerning the amount, size, position, and orientation of the microcracks.

The number of load cycles to failure tended to be slightly lower for the fiber-reinforced specimens compared to the fiber-free specimens. The strains in the axial direction of the fiber-free specimens are lower until fracture. The material degradation was investigated by means of a microscopic analysis of the microcrack development. This analysis shows that in both high-performance concrete, and fiber-reinforced high-performance concrete microcracking primarily takes place in the interfacial transition zone (ITZ), and in the hardened cement paste, the crack width changed only marginally during the applied load changes, predominantly newly formed microcracks appeared with increasing degradation. This was found in both the fiber-free and fiber-reinforced samples. The fiber-reinforced specimens show a reduced number of microcracks compared to the fiber-free specimens. Additionally, it can be concluded that the increasing degradation is essentially caused by the formation of new microcracks.

1 INTRODUCTION

Concrete is an inhomogeneous material; even minor external mechanical stresses can lead to high local stresses and, hence, structural degradation. Structural degradation in the form of microcracking can already be seen with stresses far below the static strength of the concrete. Microcracks and, thus, degradation in the microstructure increase with increasing load cycles and can cause premature failure during these stresses [1].

Micro-cracks already occur in the unloaded state, this usually takes place along the aggregate boundaries and is caused primarily by thermal and hygric incompatibilities between hardened cement stone and aggregate [2, 3]. Accordingly, the contact zone between the aggregate and the hardened cement stone (the so called "Interfacial Transition Zone" = ITZ) is a weak point in the structure. In accordance with further investigations, microcracks are usually less than 10 μm wide, and their length varies between about 50 μm and 1500 μm [3, 4]. In general, there are three phases of damage evolution of concrete that finally lead to fatigue failure, which is referred to as the "s-shaped course of fatigue". First, a significant number of microcracks are created (phase I). After this, a further steady formation of microcracks takes place (phase II), which is significantly slower than during phase I. In phase III, the crack growth increases again and there is an increased interconnection of microcracks in combination with a large increase in deformation [5]. In normal-strength concrete, microcracks are usually found in the contact zone between the aggregate and the hardened cement paste (ITZ) [6]. Currently, no clear starting point for the microcracks could be identified in high-strength concrete due to the more homogeneous structure [3]. Investigations of [7] shows, that in high-performance concretes, predominantly microcracks which connect aggregates are found. They were usually located at the smallest distance between the aggregates, so that the bond between the

aggregate and the cement paste is of considerable importance. [3]

The addition of steel fibers can improve the properties of high-performance concrete under tensile stress. The impact of fibers depends on different factors, for example, fiber geometry, fiber slenderness (length-to-diameter ratio), and fiber amount [8, 9, 10, 11, 12]. Fibers can transfer tensile stresses at least partially over the cracks after their formation and consequently improve the ductility of concrete [13]. Crack initiation is particularly crucial here, it is characterized by the interaction of individual fibers with the surrounding matrix of the hardened cement paste. Usually macrofibers ($\varnothing > 300 \mu\text{m}$) are used in the construction industry. Detrimental is, that macrofibers are activated and transmit tensile stresses only across cracks with a width greater than 50 μm . For this reason, microfibers with a diameter smaller than 100 μm should be used to effectively bridge microcracks with crack widths much smaller than 50 μm [14]. This is because in the case of microfibers with a diameter larger than 300 μm , the intact concrete ligaments still transfer the tensile stresses across the crack, and the fibers are not activated because they are too thick compared to the crack width. In order to transfer the tensile stresses across the cracks with widths smaller than 50 μm , microfibers with smaller diameters are necessary; see also [15].

2 EXPERIMENTAL INVESTIGATIONS

The influence of two different types of fibers on fatigue, strain, and microcrack characteristics is investigated in a systematic study.

2.1 Materials and composition

The investigations were carried out within the framework of the research project "Influence of microfibers on the degradation of high-performance concrete under cyclic loading," which is part of the priority program 2020 "Cyclic Deterioration of High-Performance Concrete in an Experimental-

Virtual Lab". A reference concrete composition was developed within the priority program. The investigations in the above-mentioned subproject were carried out on the high-strength reference composition (RH1). The composition is designated HPC-08 in this paper. The composition HPC-08 is characterized in [16] as a C80/95. High-strength steel fibers, designated HPC-08-SF, and carbon short fibers (HPC-08-C) were added to the composition. The compressive strengths of the specimens tested here were about 110 MPa for the HPC-08 and -08-SF. The compressive strength of the HPC-08-C was slightly lower at 100 MPa. tested on a cube-shaped test specimen with 150 mm of edge length. The respective compositions are shown in Table 1.

Table 1: Compositions

Materials		HPC		
		08	08-SF	08-C
Cement	[kg/m ³]	500		
Sand 0/0.5	[kg/m ³]	75		
Sand 0/2	[kg/m ³]	850		
Basalt 2/5	[kg/m ³]	350		
Basalt 5/8	[kg/m ³]	570		
Super-plasticizer	[kg/m ³]	5.0	7.0	
Stabilizer	[kg/m ³]	2.85	3.65	
w/c	[-]	0.35		
Fiber content	[Vol.-%]	-	1.0	0.5

The specimens were stored underwater for 28 days in accordance with DIN EN 12390-2. They were then prepared for the tests, i.e., covered with strain gauges, and tested immediately. The properties of the fibres used are shown in table 2.

Table 2: Properties of the fibers

	Strength	Length	Ø	Density
	[MPa]	[mm]	[mm]	[kg/dm ³]
Steel	2600	6	0,16	7,85
Carbon	4000	6	0,007	1,80

2.2 Experimental method and variations

The cyclic tests were performed on cylindrical specimens with a height of 300 mm and a diameter of 100 mm. This means an h/d ratio of 3 and corresponds to a typical specimen shape for fatigue tests. The slenderness of the specimens implies a relatively unimpeded transverse strain in the center of the specimen. The strains in the axial direction were continuously recorded by two strain gauges with a length of 100 mm.

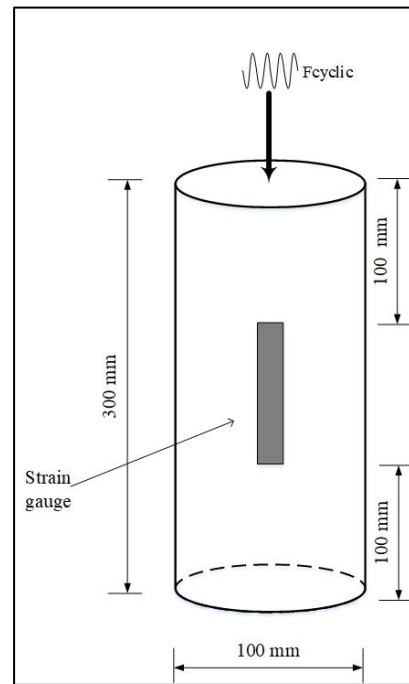


Figure 1: Schematic illustration of the specimen with strain gauge

The experiments were force-controlled. First, the compressive strength was determined on at least three specimens of each series with the same dimensions as for the fatigue tests. From this, the upper load and lower load were determined. The underload was defined as a constant 10 percent of $f_{c,max}$. The upper load varied between 45 and 70 percent of $f_{c,max}$.

After a defined number of load cycles, the respective tests were stopped, and specimens were taken for microscopic examination. So that it is possible to get knowledge about microcrack behavior after 0, 1000, 100000, and 1 million load cycles, respectively, immediately before failure.

2.3 Experimental setup

For the execution of the cyclic compressive tests, a multiple-test setup for compression tests was developed and built as part of the research project. This test setup allows three specimens to be tested under the same test boundary conditions at the same time. Since fatigue tests in particular can sometimes have a very long test duration and are generally subject to greater scatter, it is thus possible to carry out a sufficient number of fatigue tests in an adequate amount of time. The multiple test setup consists of three rigid steel frames (Fig. 2), each with a hydraulic differential cylinder with a maximum force of 1000 kN (force-controlled) and a maximum load frequency of 7 Hz. The load is applied via spherical domes with connected pressure plates. The flexible design of the test frame allows specimens with different heights and diameters to be tested. Typical dimensions for specimens in fatigue research are 300/100 mm, 180/60 mm, and 150/50 mm, corresponding to an h/d ratio of 3. [17]



Figure 2: Multiple test setup [17]

2.4 Microscopic investigations

After 0, 100,000, and 1 million load cycles, one test specimen of the three tested specimens in each series is extracted, from which thick sections were extracted, prepared and used for microscopic examinations (amount, length, width, and position of the microcracks). The thick sections were prepared with colored resin (blue) to make the microcracks as visible as possible. Two thick sections were taken out of the test specimen in the axial direction (see Figure 3). Thick sections refer to preparation

with a thickness of 200-300 μm . With the thick sections being prepared after the specimens were subjected to a different number of load cycles, it is possible to capture the crack evolution over the course of fatigue behavior.

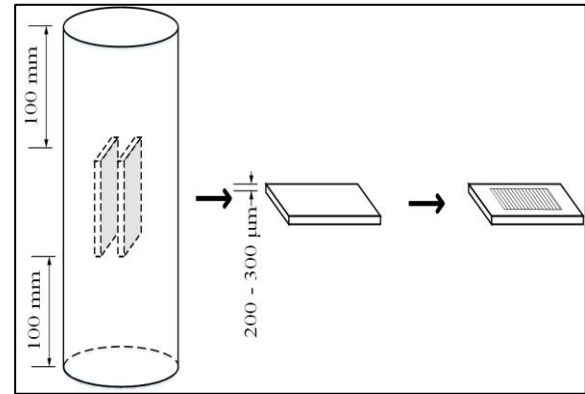


Figure 3: Examination of thick sections

3 RESULTS

The following paragraphs present the results obtained. For this purpose, the fiber-reinforced specimens are directly compared with the fiber-unreinforced reference. In addition to the maximum number of cycles to failure, the strain in the axial direction for the stress levels 0.45 and 0.70 and the microcrack characteristics are presented.

3.1 Numbers of cycles to failure

The number of cycles to failure of the high-strength composite with and without steel and carbon microfibers is presented in Figure 4 as mean values. The specimens loaded with a stress level of $S_{\text{max}} = 0.45$ all achieved the specified number of load cycles. For this reason, these tests are not shown in Figure 4. A total of 44 specimens with a maximum stress level of $S_{\text{max}} = 0.70$ were tested. For each composition, at least 14 specimens were tested to determine the mean value. The specimens were taken from different batches to ensure a comparable concrete age. The S/N curve of the 2010 model code [18] has been included for comparison.

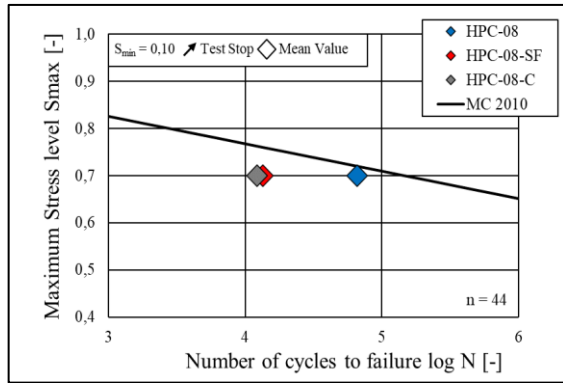


Figure 4: Number of cycles to failure for HPC-08, -SF an -C

Figure 4 shows that both the HPC-08-SF and the HPC-08-C, i.e., both compositions with fiber reinforcement, achieved lower load cycles than the unreinforced one. The values for the HPC-08-SF with $\log N = 4,13$ and the HPC-08-C with $\log N = 4,09$ were comparable. The HPC-08 achieved $\log N = 4,82$, which is slightly lower than the S/N curve according to Model Code 2010 ($\log N = 5,16$). The reason for this is that the test specimens of the investigations that are the basis for the Model Code 2010 are stored differently (and thus had different moisture conditions). The moisture condition of the specimens has a significant influence on the number of cycles to failure.

3.2 Strains

The mean strains (average of 3 specimens) at a stress level of $S_{\max} = 0,45$ are shown in Figure 5. On the x-axis, the load cycle numbers are displayed via the previously defined load cycle number. In this case, $N_F = 5$ million load cycles. At the stress level of $S_{\max} = 0,45$, no fatigue failure occurs at this number of load cycles. The strains of the fiber-free high-strength concrete (HPC-08) are lower than those of the fiber-reinforced ones. The high-strength concrete reinforced with short steel fibers shows the highest strain; the high-strength concrete reinforced with short carbon fibers shows comparable strains to the steel fiber reinforced concrete, but these strains are slightly lower.

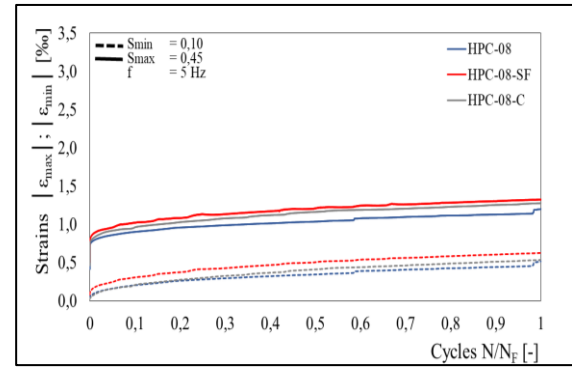


Figure 5: Averaged strains at $S_{\max} = 0,45$

At a stress level of $S_{\max} = 0,70$, the HPC-08 in phase 1 of the S-shaped damage progression initially exhibits greater denier, which then increases to a lesser extent in phase 2 compared to the fiber-reinforced specimens. For the fiber-reinforced specimens, a stronger increase in strain is then seen in phase 2. The HPC-08-C (with carbon fibers) reaches somewhat the same strain as the HPC-08 at the end of phase 3 (i.e., shortly before specimen failure). The specimens with steel fibers show larger strains shortly before specimen failure.

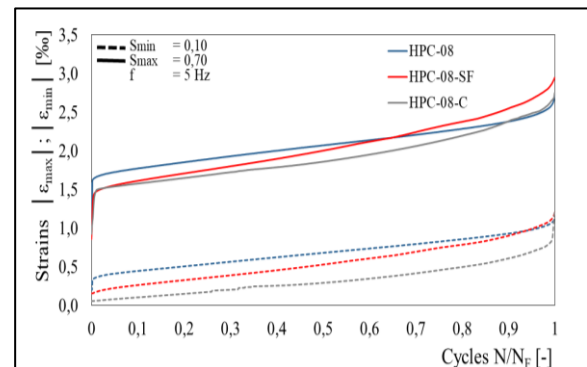


Figure 6: Averaged strains at $S_{\max} = 0,70$

The strain development is presented in the usual way for compressive fatigue behavior, with the strain development normalized to the related number of cycles N/N_F ; see Figures 5 and 6. The advantage of this representation is that differences in the shape or length of the individual phases and the absolute strain values are illustrated. A disadvantage is that the increase in strain with the increasing number of load cycles, and thus the slope of the curve, is distorted [19]. For this reason, the strain development is additionally shown for the

stress level $S_{\max} = 0.70$ in relation to the achieved number of cycles to failure, (see Figure 7).

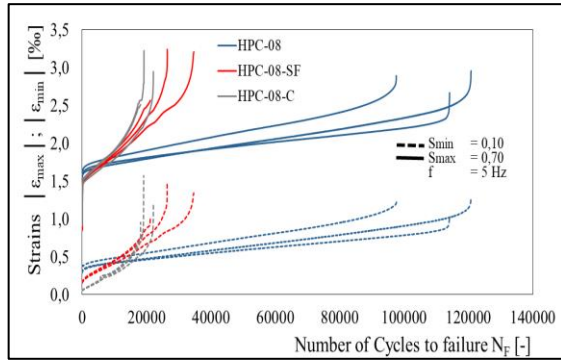


Figure 7: Strains at $S_{\max} = 0.70$ displayed via the number of cycles to failure

3.3 Crack characteristic; stress level = 0.45

The crack characteristics at a stress level of $S_{\max} = 0.45$ are shown in Table 3 for the HPC-08. The crack growth is continuous; the crack width changes initially and then remains relatively constant during the cyclic loading, between 100K and 1 million cycles. This means that at the beginning of the cyclic loading, cracks initially widen slightly, and wide cracks develop. The cracks that appear in the course of the cyclic loading then no longer show any significant change in width. Instead, new cracks of similar width are formed. The length of the microcracks changes only marginally in the course of the cyclic loading within the first 100K load cycles. After that (up to 1 million load cycles), the crack length increases. The total crack area increases by approximately 6 times after 1 million load cycles.

Table 3: Microscopic analysis of HPC-08

HPC-08	Reference	$\sigma_{\max} / f_c = 0.45$ $\sigma_{\min} / f_c = 0.10$	
		100,000	1 Mio.
Cycles	0		
Number of cracks	143	387	423
Mean crack width [μm]	4	6	6
Mean crack length [μm]	471	462	550
Total crack area [$\mu\text{m}^2/\text{mm}^2$]	111.9	482.9	640.3

In comparison, the HPC-08-C also shows an increase in microcracks in the course of cyclic loading, but the number of microcracks is significantly lower. With an average of 196 microcracks, less than half the number of microcracks as in HPC-08 can be detected after one million load cycles. In addition, the microcrack width is significantly smaller and changes only marginally as a result of the cyclic loading; the microcrack length and thus the total crack area are also significantly smaller (see Table 4).

Table 4: Microscopic analysis of HPC-08-C

HPC-08-C	Reference	$\sigma_{\max} / f_c = 0.45$ $\sigma_{\min} / f_c = 0.10$	
		100,000	1 Mio.
Cycles	0		
Number of cracks	155	218	196
Mean crack width [μm]	2	2	2
Mean crack length [μm]	341	323	370
Total crack area [$\mu\text{m}^2/\text{mm}^2$]	39.7	73.7	71.2

The high-strength concrete with steel fibers shows a microcrack development comparable to the carbon fiber-reinforced high-strength concrete in terms of the number of cracks. The overall microcrack width is larger and comparable to the HPC-08 in unloaded condition. As the cyclic loading progresses, the crack width increases slightly, but significantly less than the HPC-08. The microcrack length is the largest compared to the HPC-08 and HPC-08-C. The microcrack width is smaller in the unloaded condition. However, longer cracks appeared in this series even in the unloaded condition. The increase in crack length due to cyclic loading, however, is greatest for the HPC-08-SF without taking this into account.

Table 5: Microscopic analysis of HPC-08-SF

HPC-08-SF	Reference	$\sigma_{\max} / f_c = 0.45$ $\sigma_{\min} / f_c = 0.10$	
		100,000	1 Mio.
Cycles	0		
Number of cracks	141	202	233
Mean crack width [μm]	4	5	5
Mean crack length [μm]	534	616	630
Total crack area [$\mu\text{m}^2/\text{mm}^2$]	133.2	242.6	284.5

Table 6: Microscopic analysis of HPC-08

HPC-08	Reference	$\sigma_{\max} / f_c = 0.70$ $\sigma_{\min} / f_c = 0.10$	
		10,000	80,000
Cycles	0		
Number of cracks	128	183	274
Mean crack width [μm]	5	4	6
Mean crack length [μm]	542	564	450
Total crack area [$\mu\text{m}^2/\text{mm}^2$]	137.4	193.4	329.5

3.4 Crack characteristic; Stress Level = 0.70

At a stress level of $S_{\max} = 0.70$, the HPC-08 shows constant crack growth; see Table 6. The number of microcracks in the unloaded state is similar to that of the specimens tested at a stress level of $S_{\max} = 0.45$. Since the specimens are from different batches, it can be assumed that both tested batches had approximately the same damage state in the unloaded state. Depending on the maximum number of load cycles ($\log N = 4,82$; approx. 77K load cycles), one test was stopped at 80,000 load cycles, thus shortly before the expected failure. The microscopic evaluation after 80,000 load cycles showed a continuous increase in microcracks. However, it was noticeable that, in comparison to 100,000 load cycles applied at a stress level of $S_{\max} = 0.45$, fewer microcracks appeared. It can be concluded that not only the number of microcracks is responsible for the failure of the specimens. It is rather assumed that the abrupt failure of the specimens is due to local damage events within the specimen. This would mean that stresses can no longer be absorbed in local damage hot spots, resulting in abrupt failure starting from these points.

For the HPC-08-C at a stress level of $S_{\max} = 0.70$, the unloaded condition showed a higher number of microcracks and thus a slightly larger pre-damage to the specimen. In addition, the HPC-08-C showed significantly faster microcrack growth. After 1000 load cycles, the number of microcracks was comparable to that of the HPC-08 at 80K load cycles. After 15 K and thus shortly before failure ($\log N = 4.09$; approx. 12K load cycles) of the specimens, a similar number of load cycles of microcracks as in the HPC-08 shortly before failure of the specimens was observed.

Table 7: Microscopic analysis of HPC-08-C

HPC-08-C	Reference	$\sigma_{\max} / f_c = 0.70$ $\sigma_{\min} / f_c = 0.10$	
		1,000	15,000
Cycles	0		
Number of cracks	208	241	263
Mean crack width [μm]	1	2	2
Mean crack length [μm]	350	417	508
Total crack area [$\mu\text{m}^2/\text{mm}^2$]	45.3	85.3	87.1

At the time of writing, the microscopic analysis of the thick sections of HPC-08-SF was not yet complete.

4 DISCUSSION AND CONCLUSION

In the present paper, systematic investigations were carried out on the influence of two different fibers on the fatigue behavior of high-strength concrete. The following conclusions can be drawn from the investigations carried out:

1. Both compositions with fiber reinforcement (HPC-08-SF and -C), achieved lower load cycles than the unreinforced one (HPC-08). The Cycles to failure of the reinforced compositions were quite equal. so that there is no noticeable influence from the fiber type.
2. At a stress level of $S_{\max} = 0.45$, the strains of the fiber-reinforced concrete are larger than those of the HPC-08. This could be observed in all tested specimens. The HPC-08-SF showed the largest strains.
3. The same could be observed at a stress level of $S_{\max} = 0.70$. The HPC-08 also showed the largest strains here. Furthermore, a steeper increase in strains can be observed in the second phase of the s-shaped damage progression for the fiber-reinforced specimens.
4. Microscopic examinations of specimens subjected to cyclic loading with $S_{\max} = 0.45$ showed continuous crack growth for all compositions investigated. HPC-08 showed by far the largest number of microcracks. Regarding the crack width, the specimens with carbon fibers showed the smallest crack width and thus also a significantly smaller total crack area. The crack widths of the steel fiber-reinforced specimens were comparable to those of the unreinforced high-strength concrete.

5. At a stress level of $S_{\max} = 0.70$, the microscopic evaluation showed that the HPC-08 and HPC-08-C had approximately similar numbers of microcracks until shortly before fracture failure. The achievable number of load cycles was naturally lower in the HPC-08-C, so faster crack growth can be assumed. In this case, the microcrack width was again significantly smaller in the HPC-08-C.

On a global basis, it can be stated that the fiber-reinforced concretes investigated here exhibited poorer fatigue behavior. The maximum achievable load change was lower, and the strains were greater. With regard to the microcrack behavior, the positive effects of the fibers can be determined. The fiber-reinforced concrete exhibited fewer microcracks. The microcrack width was significantly smaller, especially in the composition with carbon fibers.

5 ACKNOWLEDGEMENTS

The authors are grateful to the German Research Foundation (DFG) for their financial support of this research project. The author is solely responsible for the content.

6 REFERENCES

- [1] Ibuk, H., 2008. Ermüdungsverhalten von Beton unter Druckschwellbelastung. Ph.D. thesis, Ruhr-Universität Bochum.
- [2] Hohberg, R., 2004. Zum Ermüdungsverhalten von Beton. PhD thesis, Technische Universität Berlin.
- [3] Kustermann, A., 2005. Einflüsse auf die Bildung von Mikrorissen im Betongefüge. PhD thesis, Universität der Bundeswehr München, Institut für Werkstoffe des Bauwesens.
- [4] Przondziono, R., Timothy, J.J., Nguyen, M., Weise, F., Breitenbücher, R., Meschke, G., Meng, B., 2015. Vorschädigung in Beton infolge zyklischer Beanspruchung und deren Auswirkung auf Transportprozesse auf eine schädigende AKR. Beton- und Stahlbetonbau, 110(1), pp. 3-12.

- [5] Thiele, M., 2015. Experimentelle Untersuchung und Analyse der Schädigungsevolution in Beton unter hochzyklischen Ermüdungsbeanspruchungen. Ph.D. thesis, Technische Universität Berlin
- [6] Tasdemir, C., 1995. Microstructural Effects on the brittleness of High Strength Concrete. *Frac-ture Mechanics of Concrete Structures (Proceedings FRAMCOS-2)*, pp. 125-134.
- [7] Guse, U., Hilsdorf, H. K., 1998. Dauerhaftigkeit hochfester Betone. Deutscher Ausschuss für Stahlbeton, Heft 487, Beuth Verlag Berlin.
- [8] Abdul-Razzak, A.A., Mohammed Ali, A.A., 2011. Modelling and numerical simulation of high strength fibre reinforced concrete corbels. *Appl. Math. Model.* 2011, 35, 2901–2915.
- [9] Jansson, A., Flansbjer, M., Löfgren, I., Lundgren, K., Gylltoft, K., 2012. Experimental investigation of surface crack initiation, propagation and tension stiffening in self-compacting steel-fibre-reinforced concrete. *Mater. Struct. Mater. Constr.*, 45, 1127–1143.
- [10] Yusof, M.A., Nor, N.M., Zain, M.F.M., 2011. Mechanical properties of hybrid steel fibre reinforced concrete with different aspect ratio. *Aust. J. Basic Appl. Sci.*, 5, 159–166.
- [11] Bhargava, P., Sharma, U.K., Kaushik, S.K., 2006. Compressive stress-strain behaviour of small scale steel fibre reinforced high strength concrete cylinders. *J. Adv. Concr. Technol.*, 4, 109–121.
- [12] Klyuev, S.V., Klyuev, A.V., Abakarov, A.D., Shorstova, E.S., Gafarova, N.G., 2017. The effect of particulate reinforcement on strength and deformation characteristics of fine-grained concrete. *Mag. Civil Eng.*, 75, 66–75.
- [13] Bentur, A., Mindess, S., 1990. *Fiber Reinforced Cementitious Composites*; Elsevier Science Publishers: Amsterdam, The Netherlands, 1990; p. 449.
- [14] Schäfer, N., Breitenbücher, R., 2019. Pull—Out tests of carbon and high-strength steel microfibres in a cement-based matrix. In *Proceedings of the fib Symposium, Krakow, Poland, 27–29 May*; Derkowski, W., Gwoździwicz, P., Hojdys, Ł., Krajewski, P., Pańtak, M., Eds.; fib: Laussane, Switzerland, pp. 1888–1895.
- [15] Kützing, L., 2002. Bruchmechanischer Ansatz zur Tragfähigkeitsanalyse von Stahlfaserbeton. *Beton Stahlbetonbau*, 97, 140–146.
- [16] Basaldella, M., Jentsch, M., Oneschkow, N., Markert, M., Lohaus, L., 2022. Compressive Fatigue Investigation on High-Strength and Ultra-High-Strength Concrete within the SPP 2020. *Materials*, 15, 3793.
- [17] Schäfer, N.; Breitenbücher, R., 2020. Influence of Aggregate on Fatigue Behavior of High-Performance Concrete Under Cyclic Loading. In: *Proceedings of the fib Symposium 2020, Shanghai, China*, pp. 781-787.
- [18] Fédération Internationale du Béton. 2013. *Fib Model Code for Concrete Structures 2010*; Ernst & Sohn: Berlin, Germany.
- [19] Hümme, J., 2018. Ermüdungsverhalten von hochfestem Beton unter Wasser. Ph.D. Thesis, Gottfried Wilhelm-Leibniz-Universität Hannover, Hannover, Germany.